Repulsive interactions between dislocations and overgrown v-shaped defects in epitaxial GaN layers

P. H. Weidlich, M. Schnedler, H. Eisele, R. E. Dunin-Borkowski, and Ph. Ebert

Repulsive interactions between dislocations and overgrown v-shaped defects in epitaxial GaN layers

P. H. Weidlich,[1] M. Schnedler,[1] H. Eisele,[2] R. E. Dunin-Borkowski,[1] and Ph. Ebert[1,a)]

[1]*Peter Grünberg Institut, Forschungszentrum Jülich GmbH, 52425 Jülich, Germany*
[2]*Institut für Festkörperphysik, Technische Universität Berlin, Hardenbergstr. 36, 10623 Berlin, Germany*

The spatial distribution and the projected line directions of dislocations intersecting a cross-sectional $(10\bar{1}0)$ cleavage plane of a GaN(0001) epitaxial layer is mapped using scanning tunneling microscopy. The data is correlated with the spatial positions of v-shaped defects. The dislocations are found to be bent away from the inclined semipolar facets of v-shaped defects, due to a strain-induced repulsive interaction. The dislocation distribution is characterized by agglomerations and intersecting bundles of dislocations with parallel projected line directions, stabilized by many body effects in the repulsive strain interactions. © 2013 AIP Publishing LLC.
[http://dx.doi.org/10.1063/1.4823474]

Group III-nitride semiconductors are a group of materials, where the applications arrived well before their defects were understood. The importance of defects arises primarily from the lack of large bulk substrates.[1] Most epitaxial layers have to be deposited on lattice-mismatched and thermal-mismatched substrates or on pseudo substrates which themselves were nucleated on mismatched substrates.[2] The mismatch induces high dislocation concentrations, which need to be reduced for improved optoelectronic applications.[3,4] A variety of methods, such as epitaxial lateral overgrowth (ELO), patterning with semipolar facets, interlayers, and 3D to 2D growth transitions, were invented to achieve a reduction of the dislocation concentration in epitaxial GaN.[5–15] The common principle for dislocation reduction is the introduction of interfaces or inclined growth facets, which influence the line directions of threading dislocations.[7,16–21]

Inclined facets are also introduced by v-shaped pits or inverted pyramidal defects typically around threading dislocations in epitaxial layers of group III-nitride semiconductors.[22–27] These v-shaped defects are delimited by six inclined $\{11\bar{2}2\}$ semipolar facets.[28] Dislocations were found to bend toward such inclined facets (produced by patterning of the substrates).[7,8,16,18,20,21,29] This attractive interaction was explained by the orientation dependent energy of dislocation lines,[19] the emergence of dislocations at inclined facets combined with the minimization of the length of the dislocation lines,[18] or/and by attractive strain effects due to image forces.[7] Recent images of the etched c growth surfaces suggest that the concentration of dislocations with c line direction component is lower in v-shaped defects than in the surrounding material.[27] This may arise from a bending of dislocation lines toward the inclined facets of the v-shaped defects with subsequent annihilation or pinning reactions during overgrowth,[30] in agreement with the above outlined models. However, the reduction of the dislocation etch pit density in the v-shaped defects may also arise from repulsive interaction not considered so far. Hence, understanding interactions of dislocations with each other and with meso scale

defects is a critical issue for the growth of low dislocation density epitaxial GaN layers.[31]

In this Letter, we investigate the interactions of dislocations and v-shaped defects by mapping their spatial distributions and projected line directions on a cross-sectional $(10\bar{1}0)$ cleavage plane of GaN(0001) epitaxial layers using scanning tunneling microscopy (STM). We identify repulsive interactions between v-shaped defects and dislocations bending away the dislocations from the v-shaped defects. In addition, many body effects in repulsive strain interactions stabilize bundles of dislocations and induce fluctuations in their density.

An investigation of the interactions of dislocations requires a simultaneous mapping of dislocation positions and line directions relative to the defects of interest. Unfortunately, this remains a difficult task thus far. STM allows, however, a simultaneous determination of the Burgers vector and projected line direction of dislocations as well as a mapping of the dislocation concentration over large fields of view.[32] In order to map dislocation positions relative to v-shaped defects by cross-sectional STM (XSTM), we utilize a n-type doping modulation along the c-(growth) direction within the epitaxial GaN layers. Such a doping modulation is easily visible in XSTM images[33] and visualizes the v-shaped defects.[28] The samples were cleaved in ultrahigh vacuum (1×10^{-8} Pa) along a $(10\bar{1}0)$ plane, opening a cross-sectional view on the epitaxial layers.[34] In order to allow an accurate measurement of distances in the measured large scan-range STM images, the distortions due to the scanning tube have been corrected using a calibration sample as described previously.[35]

Figure 1(a) shows a large scale overview mosaic consisting of three constant-current XSTM images. The [0001] growth direction is toward the top side of this cross-sectional view. The cleavage surface exhibits terraces separated primarily by monoatomic steps. Some steps abruptly terminate at dislocations intersecting the cleavage surface [see dashed circles in Fig. 1(a)].[32] Superimposed on the stepped surface, a roughly periodical contrast change arising from a doping modulation can be discerned as dark contrast lines. The orientation of the doping modulation exhibits two sharp

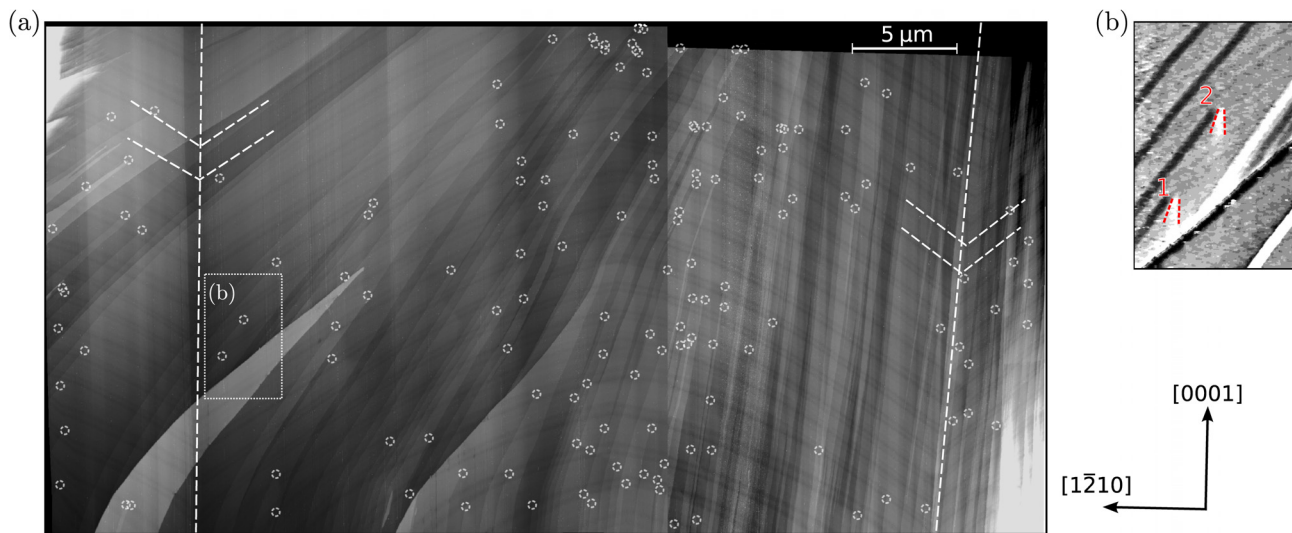a)Electronic mail: p.ebert@fz-juelich.de

FIG. 1. (a) Mosaic consisting of three constant-current STM images of a cross-sectional cleavage plane through an epitaxial GaN(0001) layer. Two v-shaped defects are visible (dashed lines). The surface consists of terraces separated primarily by monolayer high steps. At end points of steps, dislocations intersect the cleavage surface (marked by dashed circles). (b) Derivative ($-dz/dx$) image of the area (3.1 μm $\times$ 4.8 μm) marked by a dotted rectangle in (a). The straight black and white lines arise from the steps. The two dislocations exhibit a displacement field rotated by about 10° relative to the [000$\bar{1}$] direction.

v-shaped cross-sections (marked by v-shaped dashed lines) extending along the growth direction as indicated by dashed straight lines in Fig. 1(a). The v-shaped edges in the GaN epitaxial layers arise from overgrown v-shaped defects with six $\{11\bar{2}2\}$ inclined growth facets.[28]

First, we address the dislocations. Each observed dislocation induces a one monolayer (ML) high step on the $(10\bar{1}0)$ cleavage surface. The introduction of a 1 ML high step corresponds to a Burgers vector of the type $\pm a/3[11\bar{2}0]$ or $\pm a/3[\bar{2}110]$, tilted each by 30° with respect to the surface normal.[32] The STM image would also be compatible with "mixed" dislocations with an $a + c$ Burgers vector, but their concentration is significantly lower[36–38] due to the higher energy related to the longer Burgers vector.[39] Dislocations with Burgers vectors lying fully within the surface plane, e.g., along the c direction, cannot be observed in this large scale image without lateral atomic resolution. Hence, only dislocations with $a/3\langle11\bar{2}0\rangle$ Burgers vectors are observed.

Initially, such dislocations are $a/3\langle11\bar{2}0\rangle$-type threading edge dislocations with a line direction parallel to the [0001] direction. They never intersect the cleavage plane and hence would be invisible. Since we observed dislocations on our cleavage surface, their lines have been bent away from the [0001] direction. Thus, the dislocations switched from a pure edge to a mixed type. A more detailed analysis of the line direction will be performed below.

At this stage, we address the spatial distribution of dislocations with respect to v-shaped defects. The dashed circles [Fig. 1(a)] and the derived local dislocation concentration [Fig. 2(a)] show strong fluctuations. Two effects meet the eye: First, the average dislocation concentration shown in Fig. 2(b) changes by almost one order of magnitude along the [1$\bar{2}$10] direction. It reaches its maximum of about 5×10^7 cm^{-2} between the v-shaped defects. The minima occur at the centers of the v-shaped defects, whose positions are indicated by the dashed lines. Note these concentration values take only into account dislocations with $a/3\langle11\bar{2}0\rangle$-type Burgers vectors sticking out of or into the cleavage

plane. The third $a/3\langle11\bar{2}0\rangle$-type Burgers vector is lying parallel to the cleavage plane and hence is invisible in the STM images. Assuming an equal distribution of all Burgers vectors the actual dislocation concentration is likely 50% higher.

Second, the dislocation distribution in the region of high densities exhibits striking inhomogeneities along the growth direction. The dislocations form agglomerations with dimensions of 3–5 μm and consisting of 10 to 20 dislocations. The concentration in these agglomerations reaches values of
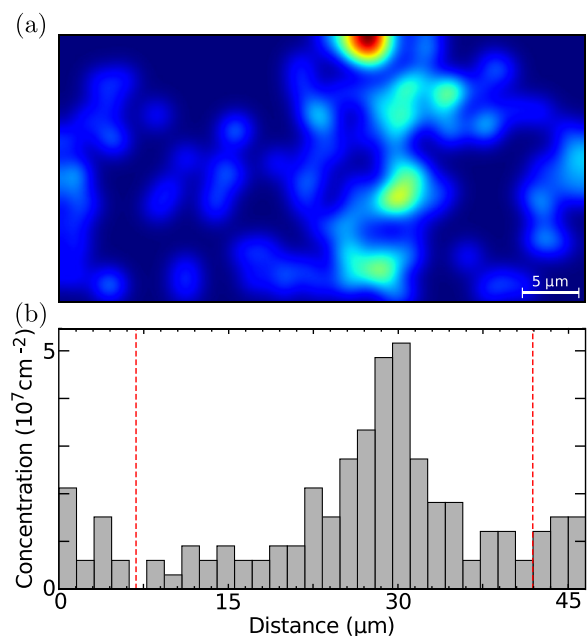
FIG. 2. (a) Local concentration of the dislocations intersecting the cleavage surface shown in the identical frame size as in Fig. 1(a). Dark blue indicates a low and bright red the highest dislocation concentration. Agglomerations of dislocations are observable. (b) Average dislocations concentration along the [1$\bar{2}$10] direction. The minimum dislocation concentration is at v-shaped defects, whose positions are indicated by dashed lines.

about $1 \times 10^8 \, \text{cm}^{-2}$. In low dislocation density areas only individual dislocations occur.

In order to understand the formation of the agglomeration, we turn to the line directions of the dislocations. Initially, their line directions are parallel to the [0001] growth direction, but with progressing growth they may bend toward non-polar directions. Since we observed dislocations intersecting the $(10\bar{1}0)$ cleavage plane, their lines have bent. The line direction can be further quantified using the displacement field visible in the STM images.[32] The displacement field of a dislocation is largest at the dislocation core and decays with distance. If a dislocation line intersects the surface with a large angle with respect to the normal direction, the displacement field of the subsurface dislocation distorts the surface anisotropically. This can be seen in the derivative image in Fig. 1(b), where the displacement field extends anisotropically downward, tracing the line direction (the diagonal contrast lines arise from steps and are not of interest). Dislocations intersecting the surface perpendicular yield a spherical displacement field.

Using this analysis, we derived the projected line direction relative to the c direction of every dislocation [Fig. 3(a)]. This is shown in Fig. 3(a), in which the angle is plotted as color-coded point at the position of the dislocation intersection with the cross-sectional surface in the frame of Fig. 1(a). Open circles represent dislocations with line directions normal to the surface (no detectable projected component). Figure 4 shows the frequency distribution of the projected line directions of the dislocations. Note, in this analysis the projected line directions in $[1\bar{2}1l]$ and $[\bar{1}2\bar{1}\bar{l}]$ directions are considered to be identical since the orientation of the dislocation line is arbitrary. The minimum at $0°$ (dislocation lines with a projected orientation along the c direction) indicates
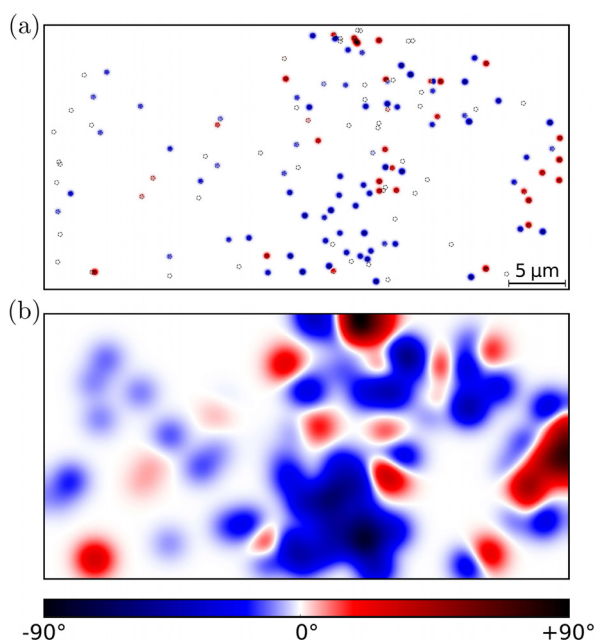

FIG. 4. Distribution of the orientations of projected line directions relative to the c direction at $0°$. All dislocations bent away from the c direction.

that most dislocations are bent. Large bending angles $> 30°$ are preferred. Note dislocations without projected component of the line direction (not included in Fig. 4) have a line direction perpendicular to the cross-sectional surface, i.e., they also have a large bending angle with respect to the c direction.

Figure 3(b) shows the average local projected line directions. The large areas of same colors indicate agglomerations of dislocations with similar projected line directions, suggesting the presence of bundles of dislocations with mostly parallel line directions.

The statistical analysis above shows that the dislocation lines are bent toward the non-polar directions. Calculations yield the lowest energy state for a $90°$ bending, resulting in a pure screw dislocation.[19] Local energy minima exist also for $45°$ bending. It can be expected that the bending reduces the energy of all dislocations with $a/3\langle11\bar{2}0\rangle$ Burgers vectors identically. Hence, dislocations with the same Burgers vector should be bent similarly, leading to bundles of parallel dislocation lines.

Neighboring parallel dislocations with the same or $60°$ rotated Burgers vectors feel repulsive interactions due to the strain field. In equilibrium, this repulsive interaction would lead to a homogeneous dislocation distribution with maximized separations. This is not observed. Hence, there has to be some attractive term. A similar problem occurred for repulsive screened Coulomb interactions between charged dopants in GaAs, which were also found to form agglomerations.[40] Many body effects in the repulsive interactions lead to effectively attractive pair interaction potentials, which induce an agglomeration. Since strain interactions have a large interaction range due to their slow decay,[41] many dislocations will interact simultaneously, too. These many body effects in the *strain* interactions may induce an effective attraction for otherwise repulsive strain interactions between the dislocation cores. This leads to inhomogeneities in the distribution of dislocations in agreement with the observed agglomerations of dislocations (Fig. 2(a)). Note some of the agglomerations consist of two intersecting bundles of dislocations with different line directions (compare Figs. 2(a) and 3(b)).

At this stage, we discuss the interaction between dislocations and v-shaped defects. In the cross-sectional view, the dislocation distribution in Fig. 2(b) peaks in between of v-shaped defects, with the lowest concentration at the v-shaped defects. This is corroborated by the reduced dislocation density at v-shaped defects found on c-oriented growth planes

FIG. 3. (a) Color coded angle of the projected line direction with respect to the c direction (at $0°$) marked at the spatial position of every dislocation. The same frame is used for display as in Fig. 1(a). Open circles represent line directions perpendicular to the surface. (b) Local average of projected line directions of the dislocations using the same color coding. The data suggest bundles of parallel dislocation lines.
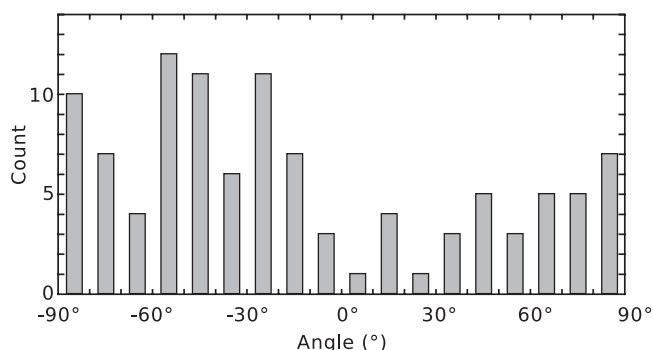
(top view).[27] The observations indicate a repulsive interaction between v-shaped defects and dislocations, resulting in a bending away from the v-shaped defect. Previously, dislocations were found to bend toward inclined semipolar facets,[7,8,16,18,20,21] i.e., in opposite direction than observed here. The origin of this effect can be traced to different strain structures: V-shaped defects in hydride vapor phase epitaxy grown GaN form typically around defect-induced growth instabilities,[11,27,42] which introduce strain fields, whereas wings in ELO are mostly free of defects and dislocations and their strain fields. Hence in ELO, the minimization of the line length and energy bends the dislocation lines *toward* the inclined facet. In contrast, the strain fields in v-shaped defects interact *repulsively* with the strain field of the surrounding dislocations and bend them *away* from inclined facets.

In conclusion, we mapped the spatial distribution and line directions of dislocations intersecting a cross-sectional cleavage surface of an epitaxial GaN layer by STM. The correlation of the dislocation distribution and line directions with the spatial positions of v-shaped defects shows that the dislocations are bent *away* from the inclined semipolar facets of the v-shaped defects, opposite to ELO wings. The repulsive interaction between dislocations and v-shaped defects is traced to strain fields. The dislocation distribution is characterized by agglomerations and intersecting bundles of dislocations with parallel projected line directions. The formation of these bundles is explained by an energy minimization driven bending and many body effects in the repulsive strain interactions.

[1]I. Grzegory, B. Łucznik, M. Boćkowski, and S. Porowski, J. Cryst. Growth **300**, 17 (2007).
[2]P. Gibart, Rep. Prog. Phys. **67**, 667 (2004).
[3]Y. Y. Enya, Y. Yoshizumi, T. Kyono, K. Akita, M. Ueno, M. Adachi, T. Sumitomo, S. Tokuyama, T. Ikegami, K. Katayama, and T. Nakamura, Appl. Phys. Express **2**, 082101 (2009).
[4]S. E. Bennett, Mat. Sci. Technol. **26**, 1017 (2010).
[5]A. Usui, H. Sunakawa, A. Sakai, and A. A. Yamaguchi, Jpn. J. Appl. Phys., Part 2 **36**, L899 (1997).
[6]O.-H. Nam, M. D. Bremser, T. S. Zheleva, and R. F. Davis, Appl. Phys. Lett. **71**, 2638 (1997).
[7]P. Vennéguès, B. Beaumont, V. Bousquet, M. Vaille, and P. Gibart, J. Appl. Phys. **87**, 4175 (2000).
[8]K. Hiramatsu, K. Nishiyama, M. Onishi, H. Mizutani, M. Narukawa, A. Motogaito, H. Miyake, Y. Iyechika, and T. Maeda, J. Cryst. Growth **221**, 316 (2000).
[9]A. Krost and A. Dadgar, Phys. Status Solidi A **194**, 361 (2002).
[10]A. Dadgar, M. Poschenrieder, J. Blasing, K. Fehse, A. Diez, and A. Krost, Appl. Phys. Lett. **80**, 3670 (2002).
[11]K. Motoki, T. Okahisa, S. Nakahata, N. Matsumoto, H. Kimura, H. Kasai, K. Takemoto, K. Uematsu, M. Ueno, Y. Kumagai, A. Koukitu, and H. Seki, J. Cryst. Growth **237–239**, 912 (2002).
[12]V. Wagner, O. Parillaud, H. J. Bühlmann, M. Ilegems, S. Gradeçak, P. Stadelmann, T. Riemann, and J. Christen, J. Appl. Phys. **92**, 1307 (2002).
[13]K. Pakuła, R. Bożek, J. Baranowski, J. Jasinski, and Z. Lilienthal-Weber, J. Cryst. Growth **267**, 1 (2004).
[14]S. Bohyama, H. Miyake, K. Hiramatsu, Y. Tsuchida, and T. Maeda, Jap. J. Appl. Phys., Part 2 **44**, L24 (2005).
[15]M. Ali, A. Romanov, S. Suihkonen, O. Svensk, S. Sintonen, M. Sopanen, H. Lipsanen, V. Nevedomsky, N. Bert, M. Odnoblyudov, and V. Bougrov, J. Cryst. Growth **344**, 59 (2012).
[16]A. Sakai, H. Sunakawa, and A. Usui, Appl. Phys. Lett. **73**, 481 (1998).
[17]O. Contreras, F. Ponce, J. Christen, A. Dadgar, and A. Krost, Appl. Phys. Lett. **81**, 4712 (2002).
[18]A. E. Romanov, P. Fini, and J. S. Speck, J. Appl. Phys. **93**, 106 (2003).
[19]S. Gradeçak, P. Stadelmann, V. Wagner, and M. Ilegems, Appl. Phys. Lett. **85**, 4648 (2004).
[20]R. Datta and C. J. Humphreys, Phys. Status Solidi C **3**, 1750 (2006).
[21]J. K. Farrer and C. B. Carter, J. Mater. Sci. **41**, 779 (2006).
[22]Z. Lilienthal-Weber, Y. Chen, S. Ruvimov, and J. Washburn, Phys. Rev. Lett. **79**, 2835 (1997).
[23]Y. Chen, T. Takeuchi, H. Amano, I. Akasaki, N. Yamada, Y. Kaneko, and S. Y. Wang, Appl. Phys. Lett. **72**, 710 (1998).
[24]T. Paskova, E. M. Goldys, R. Yakimova, E. B. Svedberg, A. Henry, and B. Monemar, J. Cryst. Growth **208**, 18 (2000).
[25]X. H. Wu, C. R. Elsass, A. Abare, M. Mack, S. Keller, P. M. Petroff, S. P. DenBaars, J. S. Speck, and S. J. Rosner, Appl. Phys. Lett. **72**, 692 (1998).
[26]A. Hangleiter, F. Hitzel, C. Netzel, D. Fuhrmann, U. Rossow, G. Ade, and P. Hinze, Phys. Rev. Lett. **95**, 127402 (2005).
[27]J. Weyher, B. Łucznik, I. Grzegory, J. Smalc-Koziorowska, and T. Paskova, J. Cryst. Growth **312**, 2611 (2010).
[28]P. H. Weidlich, M. Schnedler, H. Eisele, U. Strauß, R. E. Dunin-Borkowski, and Ph. Ebert, Appl. Phys. Lett. **103**, 062101 (2013).
[29]E. Feltin, B. Beaumont, P. Vennéguès, M. Vaille, P. Gibart, T. Riemann, J. Christen, L. Dobos, and B. Pécz, J. Appl. Phys. **93**, 182 (2003).
[30]F. Y. Meng and S. Mahajan, Phys. Status Solidi A **208**, 2666 (2011).
[31]A. Béré and A. Serra, Philos. Mag. **86**, 2159 (2006).
[32]Ph. Ebert, L. Ivanova, S. Borisova, H. Eisele, A. Laubsch, and M. Dähne, Appl. Phys. Lett. **94**, 062104 (2009).
[33]H. Eisele, L. Ivanova, S. Borisova, M. Dähne, M. Winkelnkemper, and Ph. Ebert, Appl. Phys. Lett. **94**, 162110 (2009).
[34]H. Eisele and Ph. Ebert, Phys. Status Solidi (RRL) **6**, 359 (2012).
[35]M. Schnedler, P. H. Weidlich, V. Portz, D. Weber, R. E. Dunin-Borkowski, and Ph. Ebert, Ultramicroscopy **136**, 86 (2014).
[36]X. H. Wu, L. M. Brown, D. Kapolnek, S. Keller, B. Keller, S. P. DenBaars, and J. S. Speck, J. Appl. Phys. **80**, 3228 (1996).
[37]N. Grandjean, J. Massies, P. Vennéguès, M. Leroux, F. Demangeot, M. Renucci, and J. Frandon, J. Appl. Phys. **83**, 1379 (1998).
[38]Y. Xin, S. J. Pennycook, N. D. Browning, P. D. Nellist, S. Sivananthan, F. Omnes, B. Beaumont, J. P. Faurie, and P. Gibart, Appl. Phys. Lett. **72**, 2680 (1998).
[39]D. Hull and D. J. Bacon, *Introduction to Dislocations*, 5th ed. (Elsevier, Amsterdam, 2011).
[40]Ph. Ebert, T. Zhang, F. Kluge, M. Simon, Z. Zhang, and K. Urban, Phys. Rev. Lett. **83**, 757 (1999).
[41]S. K. Mathis, A. E. Romanov, L. F. Chen, G. E. Beltz, W. Pompe, and J. S. Speck, J. Cryst. Growth **231**, 371 (2001).
[42]E. Richter, U. Zeimer, S. Hagedorn, M. Wagner, F. Brunner, M. Weyers, and G. Tränkle, J. Cryst. Growth **312**, 2537 (2010).